



# CHORUS

This is the accepted manuscript made available via CHORUS. The article has been published as:

## $^{243}\text{Am}$ neutron-induced fission cross section in the fast neutron energy range

G. Kessedjian, G. Barreau, M. Aïche, B. Jurado, A. Bidaud, S. Czajkowski, D. Dassié, B. Haas, L. Mathieu, L. Tassan-Got, J. N. Wilson, F. -J. Hamsch, S. Oberstedt, I. AlMahamid, J. Floyd, W. Lukens, and D. Shuh

Phys. Rev. C **85**, 044613 — Published 19 April 2012

DOI: [10.1103/PhysRevC.85.044613](https://doi.org/10.1103/PhysRevC.85.044613)

# $^{243}\text{Am}$ neutron-induced fission cross section in the fast neutron energy range

G. Kessedjian<sup>1)\*</sup>, G. Barreau<sup>1)</sup>, M. Aïche<sup>1)</sup>, B. Jurado<sup>1)</sup>, A. Bidaud<sup>1,7)</sup>, S. Czajkowski<sup>1)</sup>, D. Dassié<sup>1)</sup>,  
B. Haas<sup>1)</sup>, L. Mathieu<sup>1)</sup>, L. Tassan-Got<sup>2)</sup>, J. Wilson<sup>2)</sup>, F.-J. Hambsch<sup>3)</sup>, S. Oberstedt<sup>3)</sup>, I.  
AlMahamid<sup>4,5)</sup>, J. Floyd<sup>6)</sup>, W. Lukens<sup>6)</sup>, D. Shuh<sup>6)</sup>

1 CENBG, Université de Bordeaux 1, CNRS/IN2P3, Chemin du Solarium, B.P. 120, 33175 Gradignan, France

2 IPN Orsay, Université Paris-Sud, CNRS/IN2P3, 91406 Orsay, France

3 European Commission, Joint Research Centre IRMM, 2440 Geel, Belgium

4 Wadsworth Center, New York State Department of Health, Laboratory of Inorganic and Nuclear Chemistry, Albany, NY 12201, USA

5 School of Public Health, State University of New York at Albany, Rensselaer, NY 12144, USA

6 Lawrence Berkeley National Laboratory, California 94720, USA

7 LPSC, Université Joseph Fourier Grenoble 1, CNRS/IN2P3, Institut Polytechnique de Grenoble

\*Present address at LPSC [kessedjian@lpsc.in2p3.fr](mailto:kessedjian@lpsc.in2p3.fr)

**Abstract:** The existing evaluations of the  $^{243}\text{Am}$  neutron-induced fission cross section have been questioned by recent measurements performed at the GNEISS facility. In the neutron energy range from 1 to 6 MeV, the GNEISS data present deviations of more than 15% with respect to the evaluations. In order to solve this problem, we have measured this cross section in reference to three different standard cross sections. The first standard reaction used corresponds to the neutron on proton elastic scattering cross section, which is known with a precision better than 0.5 % over a wide range of neutron energies (1 meV to 20 MeV). The other two experiments were conducted in reference to the  $^{235}\text{U}(n,f)$  and  $^{238}\text{U}(n,f)$  reactions. The comparison between these three standard reactions ensures that systematic parameters have been correctly evaluated. Moreover, a sensitivity analysis of parameters and correlations of parameters is described and a complete variance-covariance matrix of the measurements is presented and discussed.

## 1 Introduction

A rather large amount of  $^{243}\text{Am}$  is present in the waste generated by current nuclear reactors.  $^{241}\text{Am}$  and  $^{243}\text{Am}$  are among the Am and Cm minor actinides and are the only isotopes that can be fully separated and extracted from spent fuel rods; they are the only nuclei for which fast neutron incineration could be seriously considered in the near future. A reliable incineration reactor can only be designed if the neutron-

induced fission cross section of  $^{243}\text{Am}$  in a fast neutron spectrum is known precisely (with better than 5% accuracy) [1]. However, in the 1 to 6 MeV neutron-energy range, the existing data show systematic and significant discrepancies. These data can be categorized into two groups as follows: the first by Knitter et al. [2], Fursov et al. [3] and Seeger et al. [4], and the second by Behrens et al. [5] Goverdovsky et al. [6] and Laptev et al. [7]. The second group finds systematically higher fission cross sections than the first group. Most of the data were obtained in reference to the fission cross section of  $^{235}\text{U}$ ; only Fursov et al. have used  $^{239}\text{Pu}(n,f)$  as a reference. The most recent data from Laptev et al. is above the current evaluation values by more than 15%. As pointed out by Talou et al. [8], the discrepancy between the two group's results seems to be related to a normalization problem.

In order to solve this controversy, we have measured the  $^{243}\text{Am}$  fission cross section in reference to the neutron-proton (n,p) elastic scattering cross section, which is known with a precision better than 0.5%, over a wide neutron-energy range of 1 MeV to 20 MeV [9,10]. This is the first time such measurements have been performed. The high precision allows us to qualify these measurements as "quasi-absolute". In addition, we have conducted measurements in reference to the  $^{238}\text{U}$  and  $^{235}\text{U}$  fission cross sections, which are known with an accuracy of 1 to 3%, in the fast neutron energy range of 0.1 MeV to 10 MeV. These data allowed us to compare the normalization procedures using three different standard reactions. This paper is organized as follows: sections 2 and 3 describe the experimental setups and the analysis according to the standard reactions chosen, section 4 presents the results in comparison with existing data and evaluations, and section 5 is devoted to the variance-covariance analysis.

## **2. Quasi-absolute neutron-induced fission cross section of $^{243}\text{Am}$ : experiment in reference to the (n,p) elastic scattering cross section**

The measurements were performed at the 7MV Van-de-Graaff of the Institute for Reference Material and Measurement (IRMM) in Belgium and at the 3.54 MV accelerator facility AIFIRA at the Centre d'Etudes Nucléaires de Bordeaux- Gradignan (CENBG), France [11]. Fast neutrons from 1 MeV to 4 MeV were produced with the  $T(p,n)^3\text{He}$  reaction using a TiT solid target. Neutrons with energies from 4 MeV to 8 MeV were produced with the  $D(d,n)^3\text{He}$  reaction using a gaseous deuterium target. In these two neutron-

energy ranges, we obtained a mono-energetic neutron beam [12]. The experimental set-up is illustrated in Fig. 1.

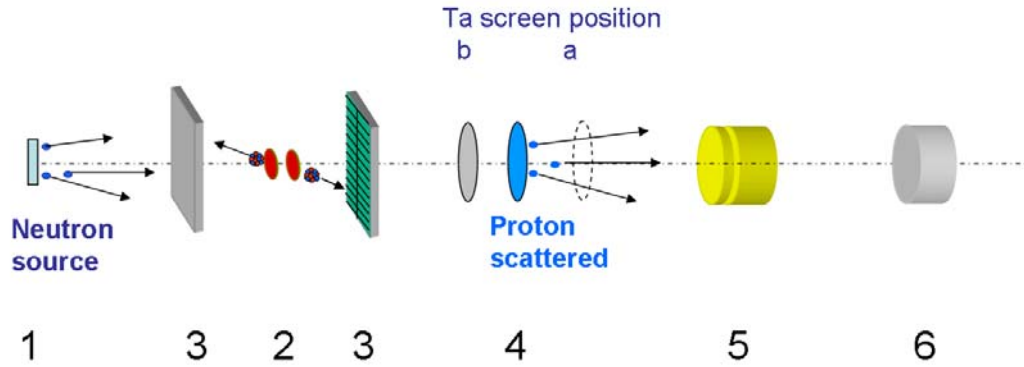


**Fig. 1.** (Color online) Experimental set-up for determining the fission cross section of  $^{243}\text{Am}$  in reference to the neutron-proton elastic scattering cross section: 1- Neutron source ( $D(d,n)$  or  $T(p,n)$  reactions). 2- Two back to back  $^{243}\text{Am}$  targets. 3- Fission fragment detectors. 4- Polypropylene foil (in blue) with the two Ta screen positions: a) background measurement or, b) neutron flux measurement. 5-  $\Delta E$ - $E$  Si telescope. 6- External  $^3\text{He}$  monitor.

Two targets of  $^{243}\text{Am}$  were placed back to back in a vacuum chamber at 39 mm from the neutron source and at  $0^\circ$  with respect to the incident neutron direction. The targets were prepared at the Lawrence Berkeley National Laboratory by electroplating techniques. The  $^{243}\text{Am}$  was deposited onto a 0.6 mm thick stainless steel backing with a deposit diameter of 6 mm; the sample thicknesses were  $546(\pm 2)\mu\text{g}/\text{cm}^2$  and  $564(\pm 2)\mu\text{g}/\text{cm}^2$ . The isotopic purity of the Am targets was  $99.96(\pm 0.01)\%$ . The target characteristics were measured by alpha spectrometry. The alpha spectrum of the targets revealed the presence of a very small quantity of  $^{249}\text{Cf}$ .

We define the  $l^{\text{th}}$  measurement of the fission cross section  $\sigma_{(n,f)}^l$  as the ratio below:

$$\sigma_{(n,f)}^l(E_n) = \frac{F_l / \Omega_l}{\Phi_n / \Omega_n}(E_n) \quad (1)$$

Where  $\Omega_l$  and  $\Omega_n$  are the solid angle of the  $l^{\text{th}}$  target of  $^{243}\text{Am}$  and the solid angle of the neutron detector, respectively,  $F_l$  is the  $l^{\text{th}}$  normalized fission rate, and  $\Phi_n$  represents the neutron flux. In the literature, almost all  $^{243}\text{Am}$  fission cross section measurements have been done in reference to  $^{235}\text{U}(n,f)$  and  $^{238}\text{U}(n,f)$ . The particularity of our new measurements is the independent normalization of our data to the well know (n,p) elastic scattering cross section, which is evaluated with a precision better than 0.5 % over a wide range of neutron energies (1 meV to 20 MeV).

## 2.1 neutron flux measurements in reference to the (n,p) elastic scattering cross section

The neutron flux measurements were done with a proton-recoil telescope. It consists of a polypropylene (PP) foil ( $(\text{C}_3\text{H}_6)_n$ ) and a silicon  $\Delta E$ -E Telescope, see Fig. 1. The PP foil (diameter:  $1.50 \pm 0.02$  cm) was placed at 80 mm from the neutron source and at  $0^\circ$  with respect to the incident neutron beam. Recoiling protons emitted from the *neutron-proton elastic scattering reaction occurring in the PP foil*, were detected at  $74.4 \pm 0.2$  mm downstream, by the silicon telescope consisting of an energy-loss detector of  $55 \mu\text{m}$  positioned in front of a residual-energy detector of  $700 \mu\text{m}$ . Several thicknesses (10 to  $50 \mu\text{m}$ ) of the PP foil were used to keep the energy loss of the recoiling protons below 15% for all incident neutron energies [15]. We define the neutron flux  $\Phi_n$  as follows:

$$\Phi_n(E_n) = \frac{N_p}{\sigma_{(n,p)} \cdot \varepsilon_p \cdot N_H \cdot \Delta t} (E_n) \quad (2)$$

Where  $N_p$  is the number of recoil protons detected with a proton detection efficiency  $\varepsilon_p$ ,  $\overline{\sigma_{(n,p)}}$  is the average n-p elastic scattering cross section for the corresponding neutron energy spectrum,  $N_H$  corresponds to the number of hydrogen atoms in the PP foil, and  $\Delta t$  is the acquisition time.

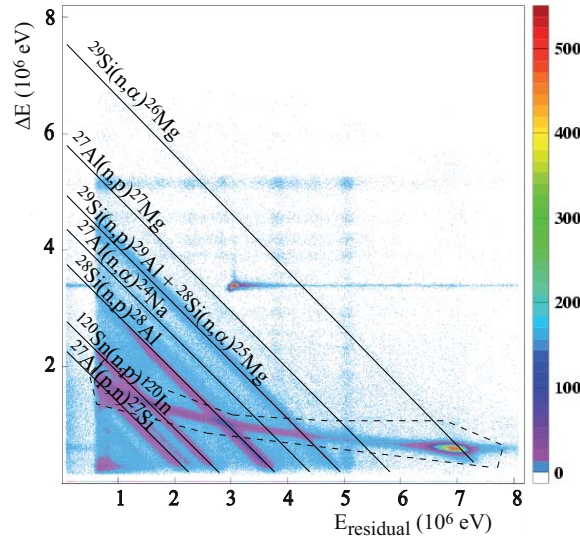


**Fig. 2.** (Color online) Light charged-particle energy loss ( $\Delta E$ ) as a function of their residual energy ( $E_{\text{residual}}$ ) detected in the silicon telescope for a 7.35 MeV incident neutron beam. The dashed line corresponds to the selection of the proton events. The background reactions in the telescope are identified

The main concern in this experiment was to perform a background subtraction of detected protons generated by neutrons scattered from the surroundings of the Telescope detector. The recoiling proton spectrum was measured at each energy with two separate measurements, namely, a standard measurement followed by a background measurement. For the standard measurement, the Telescope was in front of the polypropylene (PP) foil. For the background measurement, the recoiling protons were stopped in a tantalum screen placed between the PP foil and the Telescope, see Fig. 1. The tantalum thickness was adapted to stop the highest-energy protons. The recoiling proton events are graphically selected on a  $\Delta E$ - $E$  plot (Fig. 2). In addition to the above-mentioned background, charged particles originating from the direct interaction of neutrons with the  $\Delta E$ - $E$  Silicon were also detected by the Si-Telescope. For high neutron energies ( $E_n > 4,5$  MeV) the background is mainly due to the (n,p) and (n, $\alpha$ ) reactions within the Telescope (the silicon layers and the conducting bondings of Al and Sn). The number of protons as a function of the total kinetic energy before and after background subtraction is shown in Fig. 3. The spectrum that results from the background subtraction presents only one peak corresponding to the protons produced by the interaction of the quasi-monoenergetic incident neutrons with the PP foil. A  $^3\text{He}$

neutron monitor placed at 0 degrees with respect to the incident-neutron beam at  $4.21(\pm 0.01)$  m from the neutron source was used to normalize the standard and background measurements.

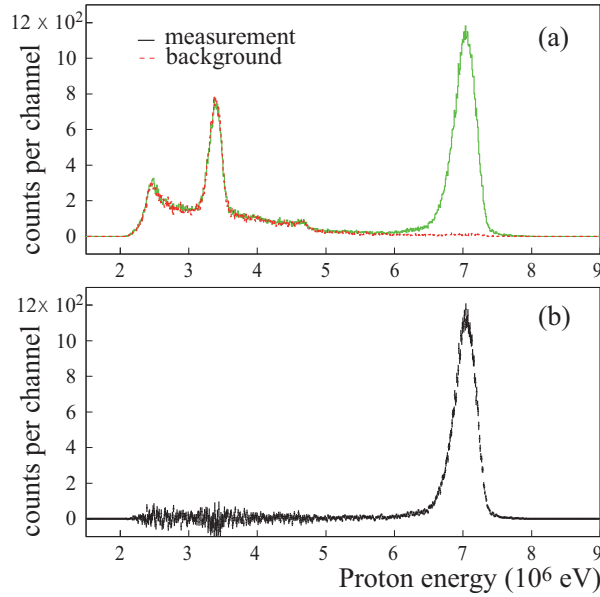


**Fig. 3.** (Color online) Number of protons detected as a function of their total kinetic energy ( $\Delta E + E$ ). (a) The standard measurement spectrum shows a pronounced proton peak around 7 MeV and a background corresponding mainly to the interaction of neutrons in the silicon Telescope. (b) Result after background subtraction. The latter shows the proton peak associated with the incident neutron flux.

In principle, the neutron flux on the PP foil is obtained by integrating the spectrum of recoil protons combined with the well known n-p elastic cross section and the telescope efficiency. By computing the ratio of the solid angles subtended by the  $^{243}\text{Am}$  targets and the PP foil we infer the neutron flux on the  $^{243}\text{Am}$  targets. However, the neutron spectrum at the PP-foil is not monoenergetic and one has to consider an average n-p cross section. Moreover, it is not obvious to determine precisely the telescope efficiency in an analytical way. For this reason, Monte Carlo simulations of neutrons and protons passing through the experimental setup have been done. They have allowed us to determine the neutron energy spectrum hitting the  $^{243}\text{Am}$  targets or the PP foil. The simulations took into account the resolution of the charged particle beam, the energy loss of the charged particle beam in the deuterium or tritium targets, the angular distributions of the neutron beam, the angular distribution of the (n,p) elastic scattering cross sections [9] [10], the proton energy loss in the PP foil, and the energy resolution of the Si telescope. When the

simulated proton spectrum is in agreement with the experimental result (Fig. 4a) it means that the simulation includes all the effects that influence the neutron path up to the PP foil as well as the tracks of recoil protons and their detection in the telescope. We can then deduce the neutron spectrum (Fig. 4b), the mean value of the (n,p) elastic scattering cross section and the proton detector efficiency as a function of neutron energy. The (n,p) elastic scattering anisotropy has been taken into account in the calculations of the proton detection efficiencies [14]. Fig. 5 shows these efficiencies for different neutron energies and for each neutron source. The results (proton spectrum and efficiency of the proton detector) of our Monte Carlo simulation code are in good agreement with the ones obtained with the code MCNPX [16].

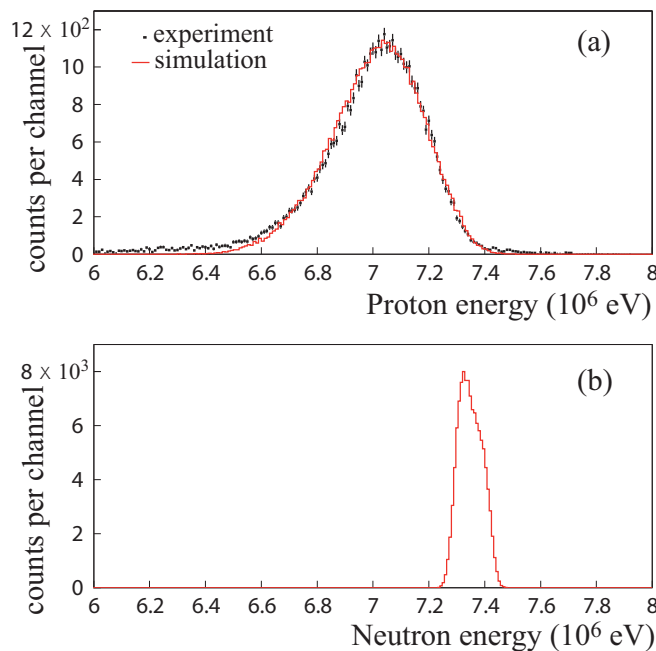


**Fig. 4.** (Color online) (a) Experimental and simulated spectra of recoil protons as a function of their kinetic energy. (b) Simulated neutron spectrum as a function of neutron kinetic energy.

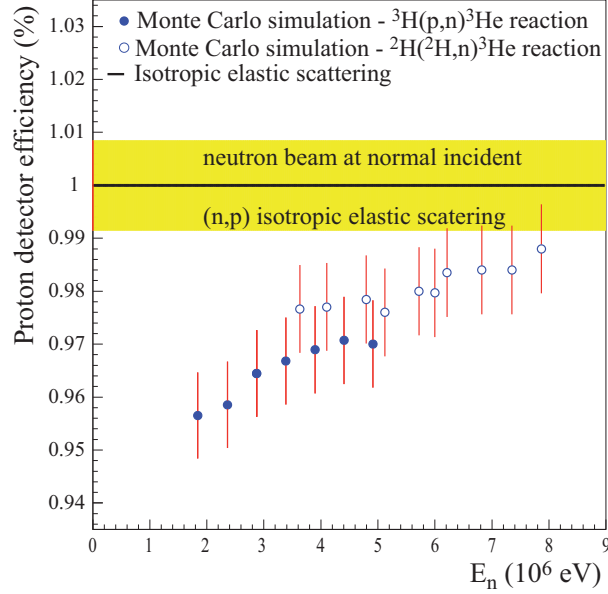


**Fig. 5.** (Color online) Simulated proton detector efficiencies as a function of neutron energy - taking into account the anisotropy of neutron emission and the anisotropy of (n,p) elastic scattering. Results are presented in comparison to isotropic proton emission and neutron beam at normal incidence (black line). The standard deviation is due to the geometrical uncertainties of the silicon Telescope (yellow area and red bars).

## 2.2- Fission rate measurements

The  $l^{\text{th}}$  normalized fission rate associated with the  $l^{\text{th}}$  target is given by the following equation:

$$F_l(E_n) = \frac{N_{ff}^l}{\mathcal{E}_{ff}^l \cdot N_{Am}^l \cdot \Delta t} (E_n) \quad (3)$$

Where  $N_{ff}^l$  is the number of fission fragments detected by the  $l^{\text{th}}$  target-detector ensemble with an efficiency  $\mathcal{E}_{ff}^l$ ,  $N_{Am}^l$  represents the number of americium atoms in the  $l^{\text{th}}$  target. As said above, we have used two  $^{243}\text{Am}$  targets for most of the measurements. The index  $l=1$  stays for the first  $^{243}\text{Am}$  target and  $l=2$  for the second one.

The fission detectors were composed of two sets of photovoltaic cells. The photovoltaic cells [13] allowed a complete separation between alpha particles and fission fragments (Fig. 6). The double humped structure was not observed in the fission fragment spectrum because the energy resolution was spoiled by

the target thickness. The photovoltaic cells have no sensitivity to the neutron beam and an intrinsic efficiency of  $95(\pm 1)$  %. Fission detectors were placed in front of each Am target in a very compact geometry to obtain a geometrical efficiency of about 70%. At neutron energies above 1 MeV, one cannot neglect kinematics effects resulting from the moving fissioning system. This is illustrated in Fig. 1 for target 1 (the detected fragments are emitted forward) and target 2 (the detected fragments are emitted backward). The efficiency plotted values correspond to fragments isotropically emitted in the Center of Mass system (Fig. 7).

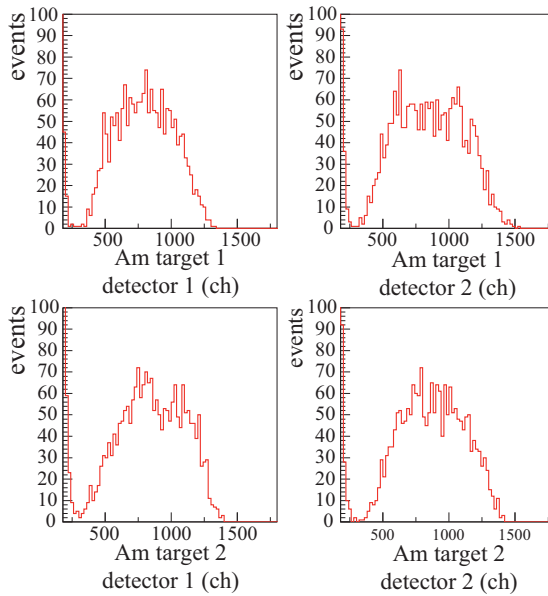


**Fig. 6.** (Color online) Fission fragment spectra for the four solar cells used in our experiments. The energy resolution allows a complete separation of alpha particles and fission fragments in the four fission detectors.

The kinematic effects and the uncertainties on geometrical parameters have been taken into account to define precisely the value and the uncertainty of the fission efficiency, which is one of the most important sources of uncertainty in this experiment. The large angular acceptance of the fission detectors implies a low sensitivity to the angular anisotropy of the fission fragments. For an anisotropy  $W(0^\circ/W90^\circ) < 1.10$ , the variations of efficiency are consistent with the standard deviations plotted on Fig. 7 [14].

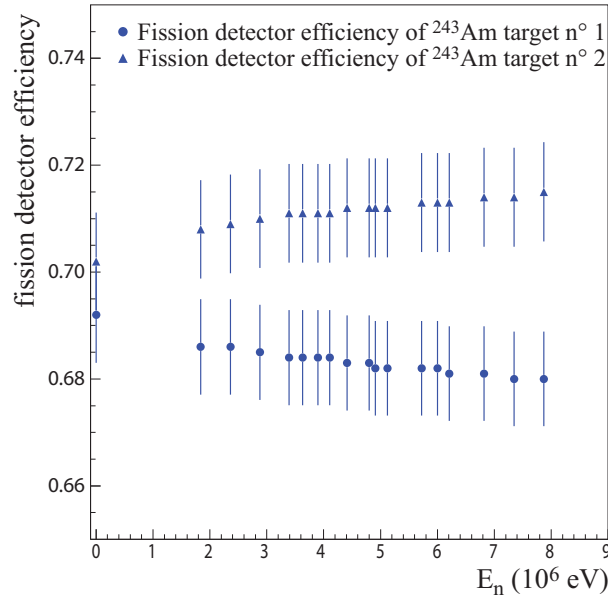


**Fig. 7.** (Color online) Simulated efficiencies of the fission fragment detectors with the kinematic correction as a function of incident neutron energy.

### 3- Neutron-induced fission cross section measurements of $^{243}\text{Am}$ relative to $^{235,238}\text{U}$

Cross-section measurements of  $^{243}\text{Am}(n,f)$  relative to  $^{238}\text{U}(n,f)$  were performed at the new 3.54 MV facility (AIFIRA) at the CENBG (see Fig. 8). The fast neutron flux with energy over the range of 4 to 6 MeV was produced by the  $\text{D}(d,n)^3\text{He}$  reaction using a deuterium gas target. Back-to-back targets, consisting of  $^{243}\text{Am}$  ( $546 \mu\text{g}/\text{cm}^2$  ( $\pm 0.5\%$ ) thick) and  $^{238}\text{U}$  ( $462 \mu\text{g}/\text{cm}^2$  ( $\pm 1.5\%$ ) thick), were placed at a distance of 40 mm from the neutron source and perpendicularly to the incident-neutron beam. The fission detectors consisted of two sets of photovoltaic cells in a very compact geometry. The ensemble “Am target + fission fragment detector” was the same as the one used for the cross section measurements relative to the (n,p) elastic scattering. The ensemble “ $^{238}\text{U}$  target + fission fragment detector” formed our second neutron flux detector. Consequently, the determination of the neutron flux was completely independent of the previous method.

The cross-section measurements of  $^{243}\text{Am}(n,f)$  relative to  $^{235}\text{U}(n,f)$  were performed at the 4MV Van-de-Graaff facility of the CENBG using the same method above (Fig. 8). For these measurements, two targets

of  $^{243}\text{Am}$  ( $106 \mu\text{g}/\text{cm}^2 (\pm 0.5\%)$ ) and  $^{235}\text{U}$  ( $409 \mu\text{g}/\text{cm}^2 (\pm 1\%)$ ) were used. Thus, these data are independent of all other measurements as shown in Table 2.

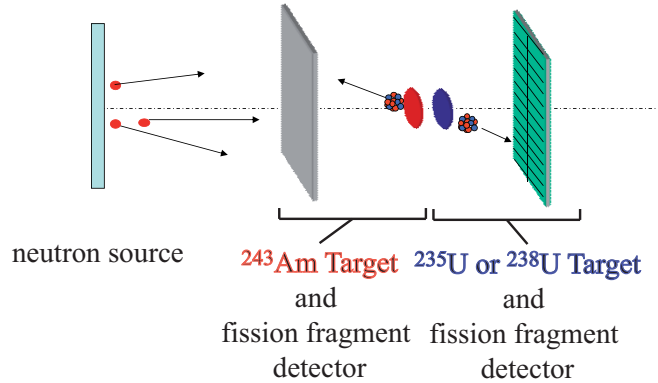


**Fig. 8.** (Color online) Experimental set-up for determining the fission cross section of  $^{243}\text{Am}$  in reference to the  $^{235}\text{U}$  and  $^{238}\text{U}$  neutron-induced fission cross sections.

#### 4- Results in comparison with experimental data and evaluations

Our results are represented in Fig. 9 in comparison with earlier measurements and the existing evaluations. In this figure the error bars of our data correspond to the maximum standard deviations, which are obtained when no solid angle correlations are considered. As can be seen in Fig.9, our measurements contradict those of Laptev [7] which are about 15 % higher than the existing evaluations. Our additional measurements (relative to  $^{235}\text{U}$  and  $^{238}\text{U}$ ) are fully compatible with these findings. Our results are in close agreement with the data of Knitter [2] as well as the evaluated data files. Table 1 presents our results including the statistical and the total standard deviations for each measurement. The latter is given without considering solid angle correlations. A complete description of our results involves a calculation of the variance-covariance matrix which will be presented in section 5.

$E_n$ (MeV)	Standard deviation on $E_n$ (MeV)	$\sigma_{(n,f)}$ (b)	Statistical standard deviation on $\sigma_{(n,f)}$ (%)	Total standard deviation on $\sigma_{(n,f)}$ (%)
Set n°1, Van de Graff, IRMM – in reference to H(n,p) – neutron source $^3\text{H}(p,n)^3\text{He}$				
1.84	0.10	1.51	1.1	3.4
2.36	0.09	1.58	1.3	3.4
2.88	0.09	1.60	1.0	3.3
2.88	0.09	1.62	0.6	3.3
3.39	0.08	1.55	0.7	3.3
Set n°2, Van de Graff, IRMM – in reference to H(n,p) – neutron source $^2\text{H}(^2\text{H},n)^3\text{He}$				
5.12	0.07	1.50	0.6	2.9
5.72	0.06	1.55	0.7	2.9
6.82	0.05	2.19	1.3	3.7
7.35	0.04	2.29	1.1	2.9
Set n°3, AIFIRA, CENBG – in reference to H(n,p) – neutron source $^2\text{H}(^2\text{H},n)^3\text{He}$				
3.59	0.20	1.59	2.4	4.6
4.07	0.12	1.60	2.1	4.5
4.77	0.07	1.54	1.5	4.2
6.00	0.05	1.64	1.8	4.4
6.21	0.04	1.82	1.9	4.4
Set n°4, Van-de-Graaff, CENBG - in reference to $^{235}\text{U}(n,f)$ - neutron source $^2\text{H}(^2\text{H},n)^3\text{He}$				
4.00	0.05	1.48	2.3	6.2
4.59	0.05	1.55	2.5	6.3
5.31	0.05	1.38	1.7	6.0
Set n°5, AIFIRA, CENBG – in reference to $^{238}\text{U}(n,f)$ – neutron source $^2\text{H}(^2\text{H},n)^3\text{He}$				
4.39	0.05	1.53	2.6	4.8
4.70	0.05	1.54	2.2	4.6
5.50	0.05	1.40	1.4	4.3
6.00	0.05	1.72	1.7	4.4

**Table 1:**  $^{243}\text{Am}$  fission cross section measurements relative to three standard reactions: (n,p) elastic scattering,  $^{235}\text{U}(n,f)$  and  $^{238}\text{U}(n,f)$ . The standard deviations are given without solid angle correlations (see part 5).

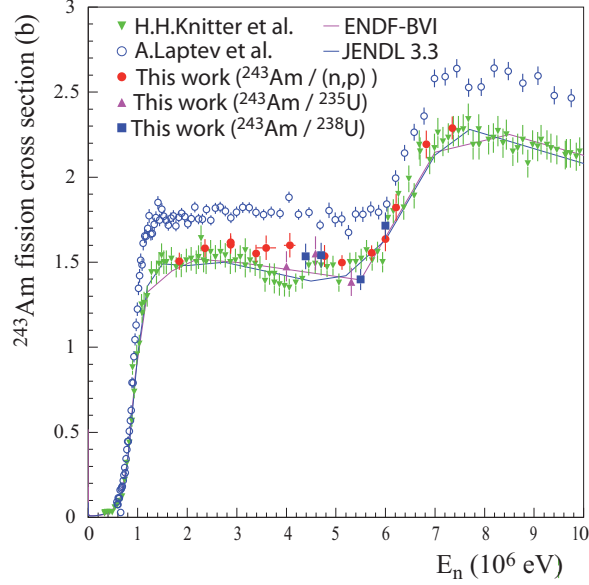


**Fig. 9.** (Color online) Results of  $^{243}\text{Am}$  neutron-induced fission cross sections in comparison with the evaluated data files and the experimental data from Knitter [2] and Laptev [7].

## 5- Variance-covariance analysis of cross section measurements

In this section we illustrate how the uncertainties and the correlation matrix for the uncertainties of the previous measurements are obtained. The latter are extremely important for evaluation purposes [17]. The variance of the measured cross section can be strongly affected by possible inter-dependency between the different parameters involved in the determination of the cross section. In addition, when cross sections are measured at different energies with the same (or partly the same) set-up, the results are not completely independent. An important particularity of this experiment for the uncertainty assessment is that for most of the energies we have used two  $^{243}\text{Am}$  targets (see Fig. 1). Accordingly, the mean fission cross section value at neutron energy  $E_i$  corresponds to the following equation:

$$\langle \sigma_{(n,f)} \rangle (E_i) = \langle \sigma_{(n,f)} \rangle_i = \frac{\langle F / \Omega \rangle}{\Phi_n / \Omega_n} (E_i) \quad (4)$$

Where  $\langle F / \Omega \rangle$  is the mean value of the  $l^{\text{th}}$  ratio  $F_l / \Omega_l$ . The index  $l=1$  stays for the first  $^{243}\text{Am}$  target and  $l=2$  for the second one. The variance-covariance study is performed in the generalized perturbation theory

framework, which assumes a linear propagation of uncertainties. Thus, the variance of the fission cross section measurement  $\langle \sigma_{(n,f)} \rangle_i$  at neutron energy  $E_i$  is given by the following equations [18]:

$$\begin{aligned}
\langle \sigma_{(n,f)} \rangle_i &= f_i(a_1; \dots; a_p; E_i) \\
\frac{Var(\langle \sigma_{(n,f)} \rangle_i)}{\langle \sigma_{(n,f)} \rangle_i^2}(E_i) &= \sum_{k=1}^p (S_{ik})^2 \frac{Var(a_k)}{(a_k)^2} + 2 \cdot \sum_{1 \leq k < k'}^p S_{ik} \cdot S_{ik'} \cdot \frac{Cov(a_k; a_{k'})}{a_k \cdot a_{k'}} \\
\frac{Cov(\langle \sigma_{(n,f)} \rangle_i; \langle \sigma_{(n,f)} \rangle_j)}{\langle \sigma_{(n,f)} \rangle_i \cdot \langle \sigma_{(n,f)} \rangle_j} &= \sum_{k=1}^p S_{ik} \cdot S_{jk} \cdot \frac{Var(a_k)}{(a_k)^2} + \sum_{1 \leq k < k'}^p (S_{ik} \cdot S_{jk'} + S_{ik'} \cdot S_{jk}) \cdot \frac{Cov(a_k; a_{k'})}{a_k \cdot a_{k'}} \quad (5) \\
\text{and } \forall k \in [1; p], S_{ik} &= \frac{\partial f_i(a_1; \dots; a_p; E_i)}{\partial a_k} \cdot \frac{a_k}{f_i(a_1; \dots; a_p; E_i)}
\end{aligned}$$

Where  $a_{k=1,p}$  are the different quantities involved in the determination of the cross section and  $Var(\sigma_{(n,f)})(E_i)$  is the variance of fission cross section measurement at neutron energy  $E_i$ ,  $Cov(\sigma_{(n,f)}(E_i); \sigma_{(n,f)}(E_j))$  is the covariance between measurement at neutron energy  $E_i$  and  $E_j$ ,  $Var(a_k)$  is the variance of the  $a_k$  parameter,  $Cov(a_k; a_{k'})$  is the covariance of the  $a_k$  and  $a_{k'}$  parameters and  $S_{ik}$  is the sensitivity of the fission cross section measurement at neutron energy  $E_i$  to the  $a_k$  parameter. The sensitivity parameters are defined without unity.

Therefore, the variance of the fission cross section measurement at neutron energy  $E_i$  is defined by the relations:

$$\text{if } \forall E_i \text{ and } \forall l, l' \in [1; m], F_l / \Omega_l \approx F_{l'} / \Omega_{l'} \text{ and } Var(F_l / \Omega_l) \approx Var(F_{l'} / \Omega_{l'})$$

$$\text{then } \frac{Var(\langle \sigma_{(n,f)} \rangle)}{\langle \sigma_{(n,f)} \rangle^2}(E_i) \approx \frac{Var(\langle F / \Omega \rangle)}{(\langle F / \Omega \rangle)^2} + \frac{Var(\Phi_n)}{(\Phi_n)^2} + \frac{Var(\Omega_n)}{(\Omega_n)^2} - \frac{2}{m} \cdot \sum_{l=1}^m \frac{Cov(\Omega_n; \Omega_l)}{\Omega_n \cdot \Omega_l} \quad (6)$$

$$\text{with } \frac{1}{Var(\langle F / \Omega \rangle)}(E_i) \approx \sum_{l=1}^m \frac{1}{Var(F_l / \Omega_l)} + \frac{2}{m^2} \cdot \sum_{0 < l < l'}^m \frac{Cov(\Omega_l; \Omega_{l'})}{\Omega_n \cdot \Omega_{l'}}$$

Where  $m$  is the number of  $^{243}\text{Am}$  targets used in the measurement (i.e.  $m = 1$  implies that the measurement was done with only one  $^{243}\text{Am}$  target and  $m = 2$  with two  $^{243}\text{Am}$  targets). In equations (1) and (2), all the parameters are independent except the solid angles of the  $l^{\text{th}}$  Am targets  $\Omega_l$  and the neutron detector  $\Omega_n$ . We can rewrite the variance on the term  $\langle F / \Omega \rangle$  like a sum of the variance without

correlation  $Var(\langle F / \Omega \rangle)_{independent}$  and the contribution of the covariances of the target solid angles  $f_c(\Omega_l ; \Omega_{l'} ; \forall l \neq l')$ :

$$Var(\langle F / \Omega \rangle) = Var(\langle F / \Omega \rangle)_{independent} + f_c(\Omega_l ; \Omega_{l'} ; \forall l \neq l') \quad (7)$$

The solid angles depend on the distance between the neutron source and the Am targets and the distance between neutron source and the PP sample. The determination of the exit point of the neutron source is subject to an uncertainty of about 0.5 mm. Therefore, in addition to the variance of each parameter, the covariances of the solid angles have to be evaluated (eqs. 6 and 7). The target solid angles and the fission-fragment detector efficiency depend also on the target surface. However, the sensitivity of the fission cross section to the target surface is only  $S = -0.003 \text{ \%/\%}$ . Since the uncertainty associated to the target surface is of about 3%, this implies a variation of the fission cross section of 0.01 %, which is considerably smaller than the total uncertainty of our results.

For all the measurements performed at different neutron energies, with the same set-up and the same neutron source, the fission cross sections are obtained using the same values of systematic parameters (those that are not subject to statistical fluctuations). In this case, only the statistical parameters are different. Therefore, the relative covariance between two measurements at neutron energies  $E_i$  and  $E_j$  of the  $^{243}\text{Am}$  fission cross section is defined as [14]:

if  $\forall E_i ; E_j$  and  $\forall l, l' \in [1; m]$  ;  $F_l / \Omega_l(E_i) \approx F_{l'} / \Omega_{l'}(E_i)$  and  $Var(F_l / \Omega_l) \approx Var(F_{l'} / \Omega_{l'})$

$$\frac{Cov(\langle \sigma_{(n,f)} \rangle_i ; \langle \sigma_{(n,f)} \rangle_j)}{\langle \sigma_{(n,f)} \rangle_i \cdot \langle \sigma_{(n,f)} \rangle_j} = \left( \frac{Var(\langle F / \Omega \rangle)}{(\langle F / \Omega \rangle)^2} \right)_{independent} + \left( \frac{Var(\Phi_n)}{(\Phi_n)^2} \right)_{syst} + \frac{Var(\Omega_n)}{(\Omega_n)^2} \quad (8)$$

$$- \frac{2}{m} \cdot \sum_{l=1}^m \frac{Cov(\Omega_n ; \Omega_l)}{\Omega_n \cdot \Omega_l} + 2 \cdot f_c(\Omega_l ; \Omega_{l'} ; \forall l \neq l')$$

Where the index “systematic” indicates that only systematic variances have been considered (without statistical uncertainties). In our case, five experiments were performed with four different neutron sources at the IRMM in Belgium and the CENBG in France.

For two measurements made with the same set-up at two different facilities, only the systematic fission rate variances and the systematic neutron flux variance have to be propagated, the solid angles being independent. The covariance of two measurements is defined by the equation:

$$\frac{Cov(\langle\sigma_{(n,f)}\rangle_i;\langle\sigma_{(n,f)}\rangle_j)}{\langle\sigma_{(n,f)}\rangle_i\cdot\langle\sigma_{(n,f)}\rangle_j} = \left( \frac{Var(\langle F \rangle)}{(\langle F \rangle)^2} \right)_{\substack{\text{independent} \\ \text{systematic}}} + \left( \frac{Var(\Phi_n)}{(\Phi_n)^2} \right)_{\text{syst}} \quad (9)$$

To compare these data, the best observable is the correlation ( $Corr$ ) of two measurements defined as the covariance divided by the square root of the product of variances. This dimensionless quantity gives the degree of independence between the data and is limited to [-1;1].

$$Corr(\langle\sigma_{(n,f)}\rangle_i;\langle\sigma_{(n,f)}\rangle_j) = \frac{Cov(\langle\sigma_{(n,f)}\rangle_i;\langle\sigma_{(n,f)}\rangle_j)}{\sqrt{Var(\langle\sigma_{(n,f)}\rangle_i)Var(\langle\sigma_{(n,f)}\rangle_j)}} \quad (10)$$

The main difficulties in evaluating equations (6) and (8) concern the assessment of the solid angle covariances but these terms are bounded in the general case:

$$\begin{aligned} \forall l, l' \in [1; m], \quad & -\sqrt{Var(\Omega_n)Var(\Omega_l)} \leq Cov(\Omega_n; \Omega_l) \leq \sqrt{Var(\Omega_n)Var(\Omega_l)} \\ & -\sqrt{Var(\Omega_{l'})Var(\Omega_{l'})} \leq Cov(\Omega_l; \Omega_{l'}) \leq \sqrt{Var(\Omega_l)Var(\Omega_{l'})} \end{aligned} \quad (11)$$

The geometry of the set-up leads us to consider only positive covariance. For these experiments, one or two  $^{243}\text{Am}$  targets have been placed in the set-up. Then, only the mean value of the solid angle correlations  $\lambda_m$  has been considered and we can rewrite equation (8) as follows:

$$\begin{aligned} \frac{Cov(\langle\sigma_{(n,f)}\rangle_i;\langle\sigma_{(n,f)}\rangle_j)}{\langle\sigma_{(n,f)}\rangle_i\cdot\langle\sigma_{(n,f)}\rangle_j} = & \left( \frac{Var(\langle F/\Omega \rangle)}{(\langle F/\Omega \rangle)^2} \right)_{\substack{\text{independent} \\ \text{systematic}}} + \left( \frac{Var(\Phi_n)}{(\Phi_n)^2} \right)_{\text{syst}} + \frac{Var(\Omega_n)}{(\Omega_n)^2} \\ & + \lambda_m \cdot \left( -\frac{2}{m} \cdot \sum_{l=1}^m \frac{Cov(\Omega_n; \Omega_l)}{\Omega_n \cdot \Omega_l} + 2 \cdot f_c(\Omega_l; \Omega_{l'}; \forall l \neq l') \right)_{\text{max}} \end{aligned} \quad (12)$$

As said above, the index m defines the number of  $^{243}\text{Am}$  target used in the set-up. Below, we use  $\lambda_m$  as a free parameter limited to the only possible positive correlation term  $0 \leq \lambda_m \leq 1$ . In the next two sections we

will discuss the impact of the solid angle correlations on the correlations of fission cross section measurements.

### 5-1- Correlation analysis of $^{243}\text{Am}(n,f)$ cross section measurements in reference to the (n,p) elastic scattering cross section

In a first step, we assume that all the parameters are independent, i.e.  $\lambda_1 = \lambda_2 = 0$ . The results are displayed in Fig. 10. For each set of measurements, we note a large correlation ( $>0.79$ ), due to the uncertainties on the solid angles and the intrinsic systematic parameters of the method: quantities of matter, (n,p) elastic scattering cross section and detector efficiencies. Between two series of measurements, only the intrinsic systematic parameters of the method have been propagated and the correlations do not exceed 0.48 (Fig. 10). In a second step, full correlation has been assumed. The limits of the fission cross section correlation matrix ( $\text{Corr}(\langle\sigma_{(n,f)}\rangle_i; \langle\sigma_{(n,f)}\rangle_j) \leq 1$ ) provide an upper limit on solid angle correlations: for one  $^{243}\text{Am}$  target ( $m=1$ ) we obtain a limit on solid angle correlation equal to  $\lambda_1 = 1$ ; for two  $^{243}\text{Am}$  targets ( $m=2$ ), the limit on the solid angle correlation corresponds to  $\lambda_2 = 0.61$  (Fig 11). The possible range of mean solid angle correlation for one or two  $^{243}\text{Am}$  target is defined by the following intervals:

$$0 \leq \text{Corr}(\langle\sigma_{(n,f)}\rangle_i; \langle\sigma_{(n,f)}\rangle_j) \leq 1 \quad \forall i, j \Leftrightarrow \begin{cases} 0 \leq \lambda_1 \leq 1 \\ 0 \leq \lambda_2 \leq 0.61 \end{cases} \quad (13)$$

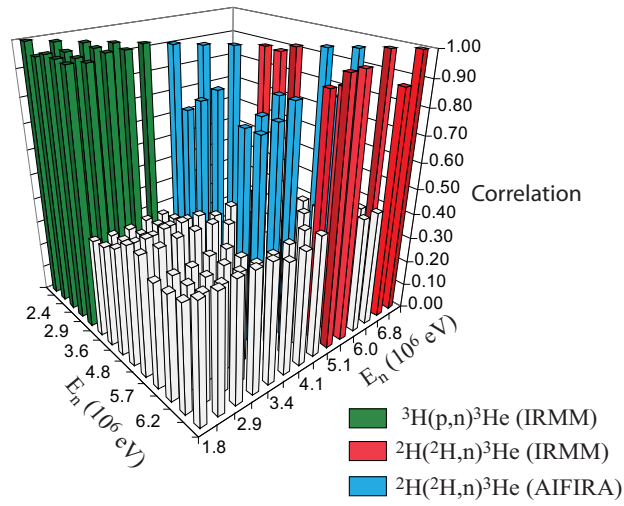


**Fig. 10.** (Color online) Correlation matrix of fission cross section measurements in reference to the  $(n,p)$  elastic scattering cross section without solid angle correlations ( $\lambda_1 = \lambda_2 = 0$ ) as a function of neutron energy ( $E_n$ ). Correlations are maximal for a same set of measurements. A significant part of correlation of uncertainties is due to the uncertainty on the position of the neutron source. Between two series, only systematic parameters of the method generate correlations.

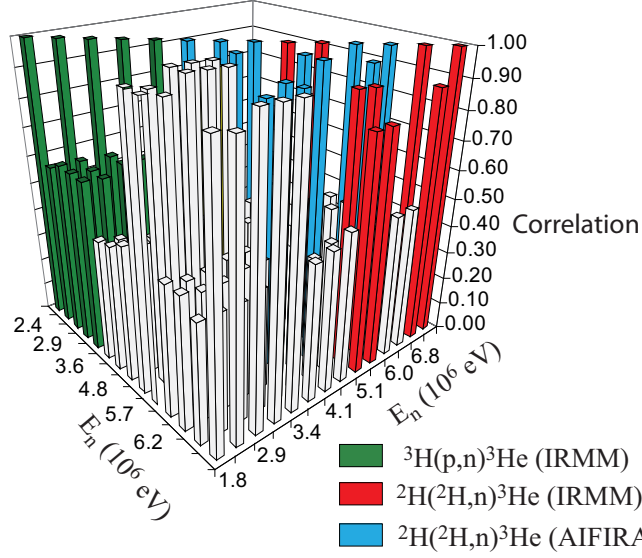


**Fig. 11.** (Color online) Correlation matrix of fission cross section measurements in reference to the  $(n,p)$  elastic scattering cross section with maximum solid angle correlations ( $\lambda_1 = 1; \lambda_2 = 0.61$ ) as a function of neutron energy ( $E_n$ ).

The fission cross section correlation matrix can be further studied as a function of the mean solid angle correlation values  $\lambda_m$  using the singular value decomposition method explained in reference [19] and presented according the following equations:

$$\begin{aligned}
 [Corr] &= [U][S][V]^T \\
 [Corr]^{-1} &= [V][S]^{-1}[U]
 \end{aligned}
 \tag{14}$$

Where  $[V]$ , respectively  $[U]$ , is composed of right singular vector  $V_i$ , respectively left singular vector  $U_i$ , associated to singular value  $S_i$ . This transformation satisfies the following equations:

$$\begin{aligned}
 UU^T &= 1 \\
 VV^T &= 1
 \end{aligned}
 \tag{15}$$

And  $[V]$  and  $[U]$  matrices are orthogonal. Each singular value represents a quasi-independent state of the matrix associated with a singular vector. This singular vector corresponds to a mix of measurements or measurement sets. This transformation provides a new representation of our data without correlation. Fig. 11 presents this decomposition for five matrices obtained by combination of two solid angle correlation

limits  $(\lambda_1; \lambda_2)$ . We observe that the singular values of five limit matrices are equivalent. Moreover, the principal singular vectors are similar and correspond to different combinations of the sets of measurements (see Table 1). The results suggest that, in our case, the variance-covariance matrix provides the same information for all solid angle correlations  $0 \leq \lambda_1 \leq 1$  and  $0 \leq \lambda_2 \leq 0.61$ . Therefore, the standard deviations of fission cross section measurements are defined by two extreme values corresponding to the extreme correlation matrices (Table 2). Finally, one can extract from the singular values the number of independent measurements without solid angle correlation ( $\lambda_1 = \lambda_2 = 0$ ) and for maximal solid angle correlations ( $\lambda_1 = 1; \lambda_2 = 0.61$ ). The number is defined as the rank of a matrix without the zero value(s). This number varies between 12 to 14 for the 14 measurements in reference to the (n,p) elastic scattering. Thus we can conclude that the solid angle correlations impact the number of independent points and have to be considered when comparing data sets from different experiments. Moreover, we can note that this analysis is needed for the generalized least square analysis used in the cross section evaluation. The inverse correlation  $[Corr]^{-1}$  (eq.14) is defined only without zero singular values.

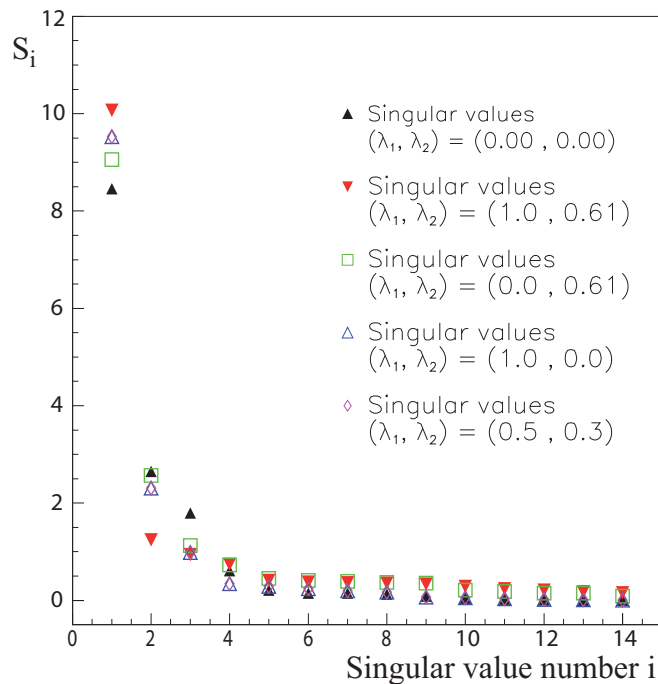


**Fig. 12.** (Color online) Singular values  $S_i$  of measurement correlation matrices as a function of the singular value number  $i=1;14$  for different solid angle correlations  $\lambda_m$ . Each value represents a quasi-independent state of the matrix. We can conclude that the information provided by the two matrices limits is similar.

In conclusion, the limits on the correlation matrix of measurements have given the limits on solid angle correlations (for the systematic variances used in this work). The limit on solid angle correlation ( $0.61 \leq \lambda_2$ ) can be interpreted as an overestimation of solid angle standard deviations. Consequently, without solid angle correlation ( $\lambda_1 = \lambda_2 = 0$ ), the standard deviation of cross section measurements is overestimated. For a maximum of solid angle correlations ( $\lambda_1 = 1; \lambda_2 = 0.61$ ), the standard deviation on cross section measurements is under-estimated. Thus, the limits on the standard deviation of measurements lie within 2.1% to 3.4% for IRMM data and 3.2% to 4.6% for AIFIRA data (Table 2). These values provide an indication of the uncertainties on the cross section standard deviations. Nevertheless, the information provided by the matrices is consistent regardless of the solid angle correlations (see Fig. 12). Finally, measurement, variances, covariances and the number of independent points provide the complete information of the experimental measurements.

$E_n$ (MeV)	$\sigma_{(n,f)}$ (b)	Minimal standard deviation on $\sigma_{(n,f)}$ (%) $\lambda_1 = 1$ ; $\lambda_2 = 0.61$	Standard deviation on $\sigma_{(n,f)}$ (%) with $\lambda_1 = \lambda_2 = 0$
Van de Graff, IRMM – in reference to H(n,p) – neutron source ${}^3\text{H}(p,n){}^3\text{He}$			
1.84	1.51	2.2	3.4
2.36	1.58	2.6	3.4
2.88	1.60	2.1	3.3
2.88	1.62	2.2	3.3
3.39	1.55	2.2	3.3
5.12	1.50	2.1	2.9
5.72	1.55	2.1	2.9
6.82	2.19	3.0	3.7
7.35	2.29	2.2	2.9
3.59	1.59	3.7	4.6
4.07	1.60	3.6	4.5
4.77	1.54	3.3	4.2
6.00	1.64	3.5	4.4
6.21	1.82	3.5	4.4
Number of independent points for measurements in reference to ${}^1\text{H}(n,p)$		14	12
Van de Graaff CENBG – in reference to ${}^{235}\text{U}(n,f)$ – neutron source ${}^2\text{H}({}^2\text{H},n){}^3\text{He}$			
4.00	1.48	5.4	6.2
4.59	1.55	5.5	6.3
5.31	1.38	5.2	6.0
AIFIRA CENBG – in reference to ${}^{238}\text{U}(n,f)$ – neutron source ${}^2\text{H}({}^2\text{H},n){}^3\text{He}$			
4.39	1.53	4.4	4.8
4.70	1.54	4.2	4.6
5.50	1.40	3.8	4.3
6.00	1.72	3.9	4.4
Total number of independent points for all measurements		21	18

**Table 2:**  ${}^{243}\text{Am}$  fission cross section measurements relative to three standard reactions: (n,p) elastic scattering,  ${}^{235}\text{U}(n,f)$  and  ${}^{238}\text{U}(n,f)$ . The measurement standard deviations are given for a maximal solid angle correlations ( $\lambda_1 = 1$  ;  $\lambda_2 = 0.61$ ) and without solid angle correlation ( $\lambda_1 = \lambda_2 = 0$ ).

**5-2- Correlation analysis of  $^{243}\text{Am}(n,f)$  cross section measurements in reference to  $^{235,238}\text{U}(n,f)$  cross sections and  $(n,p)$  elastic scattering cross section.**

The correlation within a same set of measurements is defined between 0.53 and 0.87, while the correlations between two sets of measurements do not exceed 0.17. The latter value is due to the systematic uncertainties on the  $^{243}\text{Am}$  fission rates. Correlations of the data in reference to the  $^{235}\text{U}(n,f)$  cross section with other series are equal to zero as there were no common parameters between these data. Table 3 details the correlations of these measurements (without solid angle correlations,  $\lambda_1 = \lambda_2 = 0$ ).

The measurements in reference to the  $(n,p)$  elastic scattering cross section, per group mean values of the correlation are also reported in Table 3.

Standard reaction		$^{243}\text{Am}(n,f) / (n,p)$			$^{243}\text{Am}(n,f) / ^{235}\text{U}(n,f)$			$^{243}\text{Am}(n,f) / ^{238}\text{U}(n,f)$			
		set n°1	set n°2	set n°3	4.00	4.59	5.31	4.39	4.70	5.50	6.00
$^{243}\text{Am}(n,f) / (n,p)$	set n°1	0.98	0.41	0.46	0			0.14			
	set n°2	0.41	0.84	0.46				0.10			
	set n°3	0.46	0.46	0.95				0.16			
$^{243}\text{Am}(n,f) / ^{235}\text{U}(n,f)$	4.00	0			1	0.85	0.89	0			
	4.59				0.85	1	0.88				
	5.31				0.89	0.88	1				
$^{243}\text{Am}(n,f) / ^{238}\text{U}(n,f)$	4.39	0.14	0.10	0.16	0			1	0.53	0.80	0.81
	4.70							0.53	1	0.59	0.58
	5.50							0.80	0.59	1	0.87
	6.00							0.81	0.58	0.87	1

**Table 3.** Complete description of the correlation matrix of  $^{243}\text{Am}$  fission cross section measurement for different neutron flux normalizations. For the measurement in reference to the  $(n,p)$  elastic scattering cross section, only per group mean values of correlations have been indicated for easier reading of the table.

*The results are obtained without solid angle correlation. The neutron energies related to data sets 1, 2, and 3 of the measurement in reference to the (n,p) reaction are given in Table 1.*

## **6. Conclusion**

We have presented the first measurement of the neutron-induced fission cross section of  $^{243}\text{Am}$  relative to the neutron-proton elastic scattering cross section, 14 points between 1 MeV and 8 MeV were measured. Additional measurements were made relative to  $^{238}\text{U}(n,f)$  ( 4 points) and  $^{235}\text{U}(n,f)$  (3 points). The overall precision of our data is better than 5% for the measurements done in reference to the (n,p) and the  $^{238}\text{U}(n,f)$  reactions (the statistical uncertainty is about 1 to 2% depending on the measurements). However, for the measurements performed in reference to the  $^{235}\text{U}(n,f)$  reaction, the error associated to the solid angles of the fission detectors was larger leading to higher total uncertainties (up to 6.3%). The agreement between all these measurements and the per group independency of our data validate our normalization methods and corroborate the evaluated data files. Our measurements are in agreement with those of Knitter [2] and the data libraries.

## **Acknowledgments**

This work was supported by the CNRS PACE/GEDEPEON program and the EURATOM NUDAME Transnational Access Program. We thank the IPN Orsay for building the high-quality Si detector. The authors also thank the accelerator staff of the IRMM-Geel and CENBG for their great support during the experiments. We thank E. Huffer for her help with English language.

The work at LBNL was supported by the Director, Office of Science, Office of Basic Energy Sciences, Division of Chemical Sciences, Geosciences, and Biosciences of the U.S. Department of Energy under Contract No. DE-AC02-05CH11231.

## **References**

1. M.Salvatores et al., Nuclear Science NEA/WPEC 26
2. H. H. Knitter et al., Nucl. Sci. Eng. 99 (1988)
3. B.I.Fursov et al., Atomnaya Energiya. Vol59. p339 (1985)

4. P. A. Seeger et al., "Fission Cross Sections from Pommard", LA-4220, 138, Los Alamos National Laboratory (1970).
5. J.W. Behrens, J.C. Browne, NSE, 77, 444 (1981)
6. A. A. Goverdovsky et al., Proc. Int. Conf. Nuclear Data for Basic and Applied Science, Santa Fe, New Mexico, USA, May 13–17, 1985.
7. A. B. Laptev et al., Nucl. Phys. A 734 (2004) E45.
8. P. Talou. et al., Nucl. Sci. Eng. 155 (2007) 84.
9. J.C Hopkins and G. Breit, Nucl. Data Tables, A9 (1971) 137.
10. G. M. Hale and A. S. Johnson, Proc. 17th Int. IUPAP Conf. on Few-Body Problems in Physics, 5-10 June 2003. Durham NC. W.Gloeckle and W. Tornow. eds.. Elsevier B.V., pp. S120-S122 (2004).
11. M.Aiche. G.Kessedjian et al., International Conference on Nuclear Data for Science and Technology, France, 2007.
12. M. Coppola and H.-H Knitter, Kerntechnik, Isotopentechnik und – chemie, Verlag K. Thieme KG (1967) p. 459-470.
13. G.Siegert. Nucl. Instr. and Meth., 164 (1979) 437.
14. G.Kessedjian, Ph.D thesis, Université de Bordeaux, France (2008).
15. C.Grosjean, Ph.D thesis, Université de Bordeaux, France (2005).
19. Numerical recipes, William H.Press et al., Cambridge University Press (1986).
16. <https://mcnpx.lanl.gov/>
17. T. Kawano et al., Nuclear Data Sheets 109 (2008) 2817–2821.
18. D.L Smith, Probability, statistics, and data uncertainties in nuclear science and technology, vol.4, OECD, 1991.